Raman Studies of Methane−Ethane Hydrate Metastability

Hiroshi Ohno, Timothy A. Strobel, Steven F. Dec, E. Dendy Sloan, Jr., and Carolyn A. Koh*

Center for Hydrate Research, Colorado School of Mines, Golden, Colorado 80401

Received: February 5, 2008; Revised Manuscript Received: December 21, 2008

The interconversion of methane−ethane hydrate from metastable to stable structures was studied using Raman spectroscopy. **sI** and **sII** hydrates were synthesized from methane−ethane gas mixtures of 65% or 93% methane in ethane and water, both with and without the kinetic hydrate inhibitor, poly(*N*-vinylcaprolactam). The observed faster structural conversion rate in the higher methane concentration atmosphere can be explained in terms of the differences in driving force (difference in chemical potential of water in **sI** and **sII** hydrates) and kinetics (mass transfer of gas and water rearrangement). The kinetic hydrate inhibitor increased the conversion rate at 65% methane in ethane (**sI** is thermodynamically stable) but retards the rate at 93% methane in ethane (**sII** is thermodynamically stable), implying there is a complex interaction between the polymer, water, and hydrate guests at crystal surfaces.

1. Introduction

Gas hydrates (also called clathrate hydrates) are generally formed at low temperatures and high pressures and are comprised of water cage structures which enclathrate guest gases of the appropriate size and shape.[1] Natural gas hydrate formation can cause blockages in subsea gas and oil flow lines, which can lead to catastrophic economic and safety concerns.[2] Therefore, the prevention and removal of gas hydrates during natural gas and oil subsea production and transportation are major concerns of the energy industries.[3−5]

Most gas hydrates crystallize into one of the two cubic systems, hydrate structure **I** (**sI**) and structure **II** (**sII**).[1] A unit cell of **sI** consists of 46 water molecules that form 2 pentagonal dodecahedra with 12 pentagonal faces (5^{12}) and 6 tetrakaidecahedra with 12 pentagonal faces and two hexagonal faces ($5^{12}6^2$). A unit cell of **sII** comprises 136 water molecules that form 16 5^{12} cages and 8 hexakaidecahedra with 12 pentagonal faces and 4 hexagonal faces ($5^{12}6^4$). The two main constituents of natural gases are methane and ethane, which account for more than 93% of the average gas composition.[1] Pure methane and pure ethane each form **sI** hydrate. **sI** hydrate is also formed from methane−ethane mixtures containing approximately up to 75% methane and above 99% methane. Conversely, **sII** hydrate is formed from methane−ethane mixtures containing approximately between 75% and 99% methane.[6] This interesting phenomenon was predicted theoretically by Hendriks et al.[7] and later confirmed by Subramanian et al.[8,9] using NMR and Raman spectroscopy. The **sI** to **sII** transition can be explained by considering the relative stabilities of methane and ethane in the cages of the two hydrate structures along with the ratio of large to small cavities present in each unit cell. At high ethane concentrations, **sI** is the thermodynamically favored phase as ethane preferentially occupies the larger $5^{12}6^2$ cavities, rich in **sI** (3 $5^{12}6^2$:1 5^{12}). As the composition of methane is increased, the transition to **sII** occurs due to the abundance of methane and the large number of small cavities (2 5^{12}:1 $5^{12}6^4$) in **sII** in which occupation by ethane is unfavorable. This trend causes **sII** to be the incipient hydrate phase for progressively higher concentrations of methane, until reaching very high concentrations of methane (see refs 10 and 11 for more details). At gas compositions close to the **sI/sII** transition points, the two structures usually coexist as a metastable state.[9,12,13]

Understanding the nature of the methane−ethane hydrate metastability is an important problem for the gas and oil industry because the formation of a **sI** and **sII** mixture and subsequent interconversion from a metastable to a stable structure are likely to occur in pipelines. Information which is essential for the pipeline flow assurance industry, such as dissociation pressure (or temperature) and heat capacity of the hydrate, are strongly dependent on crystal structure.[1] As another example of industrial importance, if a kinetic hydrate inhibitor is designed for **sII** inhibition, but **sI** is the predominant, metastable, hydrate former, then the inhibitor may prove ineffective. However, there have been no previous studies reported that have investigated these phenomena quantitatively. In this work, we have quantified the degree of the methane−ethane hydrate metastability at two gas compositions of 65% and 93% methane in ethane as a function of time using Raman spectroscopy. The influence of a kinetic hydrate inhibitor poly(*N*-vinylcaprolactam) (PVCap), a water-soluble polymer for gas hydrate inhibition,[14] has been investigated.

2. Experimental Methods

Hydrate Samples. Methane−ethane hydrates were synthesized in a high-pressure cell with 1 cm^3 capacity and a sapphire window of diameter 1.5 cm (Figure 1). The evacuated cell was half-filled with deionized water without and with 0.008 wt % PVCap (supplied as a 40% solution in ethylene glycol, BASF). The filled cell was then charged with the methane−ethane gas mixture of 93 mol % methane (C1) at 8.4 MPa or 65 mol % C1 at 5.3 MPa. The gas mixtures were prepared by mixing pure methane (Matheson Tri Gas) and ethane (Airgas) gases in a reservoir connected to the cell. Fresh samples were prepared for each experiment. The sample system was then cooled from 20 to 1 °C at a rate of 0.3 °C/min by circulating liquid coolant through a metal jacket surrounding the cell. The sample was maintained at this constant temperature for the remainder of the experiment. The temperature was monitored using a thermocouple placed in a hole in the brass wall of the cell. At the two gas composition and gas pressure conditions used,

* To whom correspondence should be addressed. Phone: 303-273-3237. Fax: 303-273-3730. E-mail: ckoh@mines.edu.

10.1021/jp8010603 CCC: $40.75
Published on Web 02/11/2009

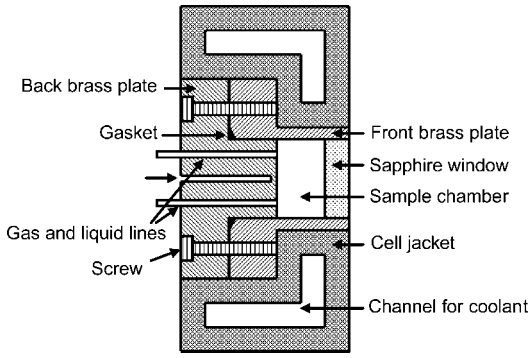

Figure 1. Schematic of the high-pressure Raman cell.

hydrate dissociation temperatures are 15 °C. Therefore, the subcooling applied to the samples was 14 °C for all cases. The sample system was allowed to stand without agitation during measurement. Because gas consumption due to hydrate formation was small, significant pressure drop and gas composition changes were not observed during the experiments.

Raman Measurements. Raman spectra of the samples were obtained using a Renishaw MK III spectrometer equipped with a 2400 g/mm grating and a multichannel CCD detector.[15,16] The gas−hydrate (or gas−water) interface was analyzed to simplify the system observed. Below the gas−water interface, gas fractionation may occur due to difference in gas diffusivity though water or hydrate phase between methane and ethane, resulting in a different stable hydrate composition. At the gas−hydrate interface, the gas diffusion process is not important, and thus we can simply assume local equilibrium at the given gas pressure and composition. The laser source (wavelength of 514.5 nm) was focused to a diameter of approximately 5 μm using a long-working-distance objective lens (Olympus SPlan 20×). The laser focal spot was first set in the gas phase at random and then was lowered to the point where gas Raman signals suddenly decrease in intensity while hydrate (or water) signals appear (the location of the measurement was not chosen by visual observation of the interface using an optical microscope). Backscattered light was corrected with the objective lens and was sent to the spectrometer through an optical fiber system. Raman frequencies were calibrated by using neon emission lines.

The induction time for hydrate formation was measured as the time at which the first hydrate signal is observed spectroscopically after the temperature dropped to 1 °C. After the hydrate nucleation, the gas−hydrate interface was measured as a function of time. Because the distribution of the hydrate structure was found to be spatially nonuniform, the laser focal point was changed (below the gas−hydrate interface) for each measurement following the procedures described above to obtain the overall structural feature of a sample. The data acquisition time for one measurement was from 30 to 180 s, depending on the intensity of the Raman scattering. Initially, hydrate structures were monitored for 6 h after the first hydrate crystals were observed. When a hydrate sample had not reached its equilibrium state (equilibrium structure) within the 6 h measurement period, further long-term observations of up to 1 week were performed. Approximately 100 independent Raman measurements were performed on a given sample. To confirm reproducibility of the observations, the induction time and Raman measurements were repeated once for each system with a fresh sample (8 observations in total; 4 systems × 2).

Reference Spectra. Figure 2 shows Raman spectra of the methane−ethane gas mixtures and hydrates, which were obtained as reference data. The hydrates were synthesized from

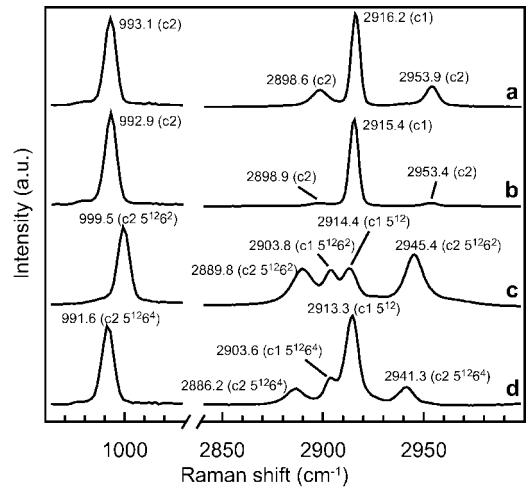

Figure 2. Raman spectra of the C−C stretching mode (~1000 cm^{-1}) and C−H stretching mode (~2900 cm^{-1}) regions at 1 °C: (a) methane−ethane gas mixture of 65% CH_4 at 5.3 MPa; (b) methane−ethane gas mixture of 93% CH_4 at 8.4 MPa; (c) methane−ethane structure **I** hydrate formed from the gas mixture a; (d) methane−ethane structure **II** hydrate formed from the gas mixture b. The hydrate spectra were taken about 1 week after the crystal nucleation. The peak assignments are based on Subramanian et al.[8,9]

the gas mixtures and deionized water using the procedure described above. To eliminate signals from the gas phase, hydrate-phase positions approximately 1 mm below the gas−hydrate (or above the gas−water) interfaces were measured. The hydrate spectra were recorded about 1 week after the first hydrate nucleation was observed. Gas-phase methane (Figure 2a and b) has a C−H stretching mode at around 2915 cm^{-1}.[8,9] Gas-phase ethane (Figure 2a and b) has a C−H stretching mode which splits into two bands due to coupling with one of the CH_3 deformation modes at approximately 2899 and 2953 cm^{-1} and a C−C stretching mode at approximately 993 cm^{-1}.[8,9] These bands shift and split when the gas molecules are enclathrated by the host water molecules (Figure 1c and d).[8,9,17] The statistical thermodynamics program CSMGem[18] was used to predict that the structure **I** hydrate is stable in the 65 mol % CH_4 sample, while the structure **II** crystal is stabilized in the 93 mol % CH_4 sample. As predicted, the hydrate spectra of the 65% CH_4 sample (Figure 2c) and that of the 93% CH_4 sample (Figure 2d) agree well with the previously reported Raman spectra of methane−ethane structure **I** hydrate and that of methane−ethane structure **II** hydrate, respectively.[8,9] Peak assignments for the **sI** and **sII** methane−ethane hydrates based on our previous work[8,9] are shown in Figure 2.

Spectra Analysis. The hydrate structures of the samples were determined by analyzing the higher-frequency ethane C−H band. This band is optimum for peak-fitting analysis because the Raman frequencies of this band differ by several cm^{-1} between the gas phase and the two hydrate structures, and this mode does not overlap with other bands in the spectra (Figure 2). Figure 3 shows examples of spectra recorded in this study and the results of the peak-fitting analyses. Deconvolution of the peaks was performed using a commercial peak-fitting program (GRAMS/AI, Galactic Industries). Peak-fitting parameters of the ethane band were obtained from the reference spectra (Figure 2 and Table 1). These parameters were constrained for all subsequent spectral deconvolutions. Hydrate structural composition can be related to the Raman peak area contribution of C_2H_6 in the $5^{12}6^4$ cavities, $I_{C2,5^{12}6^4}$, and that in the $5^{12}6^2$ cavities, $I_{C2,5^{12}6^2}$, according to the following equation, under the

assumption that the scattering cross sections of C_2H_6 molecules are independent of the type of surrounding water cage

$$V_{h,sII} = \frac{\left(\frac{I_{C2,5^{12}6^4}}{N_{5^{12}6^4}\theta_{5^{12}6^4,C2}}\right)}{\left(\frac{I_{C2,5^{12}6^2}}{N_{5^{12}6^2}\theta_{5^{12}6^2,C2}} + \frac{I_{C2,5^{12}6^4}}{N_{5^{12}6^4}\theta_{5^{12}6^4,C2}}\right)} \quad (1)$$

where $V_{h,sII}$ is the volume fraction of structure **II** hydrate in the hydrate phase; $N_{5^{12}6^2}$ and $\theta_{5^{12}6^2,C2}$ are the number concentration and ethane occupancy of $5^{12}6^2$ cavities in **sI** hydrate, and $N_{5^{12}6^4}$ and $\theta_{5^{12}6^4,C2}$ are those of $5^{12}6^4$ cavities in **sII** hydrate, respectively. $N_{5^{12}6^2}$ and $N_{5^{12}6^4}$ values calculated from crystal structures[1] are 3.47 and 1.55 nm^{-3}, respectively. The CSMGem program[18] was used to estimate that $\theta_{5^{12}6^2,C2}$ and $\theta_{5^{12}6^4,C2}$ values are 0.77 and 0.94, respectively, in the 65% CH_4 sample and are 0.28 and 0.69, respectively, in the 93% CH_4 sample. By using eq 1, the N_i and θ_i values, and the results of the peak-fitting analyses, we calculated the hydrate structural composition.

For the calculations, the distributions of guest molecules in crystals were assumed to be in the equilibrium states. This assumption is supported by our recent NMR experiment.[19] Reformation of methane−ethane hydrate from liquid water and the particular gas mixture was observed for 1 day at intervals of several minutes with the MAS NMR technique. In this experiment, the methane−ethane hydrate cage occupancy ratios were found to be almost the same as those predicted by a statistical thermodynamics program CSMGem,[18] suggesting that there is no preferential formation of large or small cages on the time scale of the NMR experiment, which is similar to that of the Raman experiment. Although a previous NMR study on Xe hydrate[20] showed that the cage occupancy of the hydrate during formation was significantly different from that in an equilibrium state, the anomaly of the cage filling was observed at the very early stage of the reaction (during a few minutes after hydrate nucleation). If such a fast phenomenon occurs in our experiment, it will not be observed because of the relatively long time scale of this Raman measurement.

To evaluate the accuracy of the Raman-shift measurement, the methane−ethane gas mixture (75% C1, 6.9 MPa, and 1 °C) was measured 30 times. The laser focal point was changed for each observation, but the position of a diffraction grating of the spectrometer was fixed in position throughout the observations, similar to the hydrate measurements. The standard deviation of peak position of the higher-frequency ethane band, which was used for the hydrate composition analysis, was 0.034 cm^{-1}, showing that the maximum experimental error of Raman shifts is about ±0.07 cm^{-1} (2σ). Assuming that ±0.07 cm^{-1} represents the maximum errors in the hydrate Raman shifts, the uncertainty of hydrate structural compositions was estimated for each measurement.

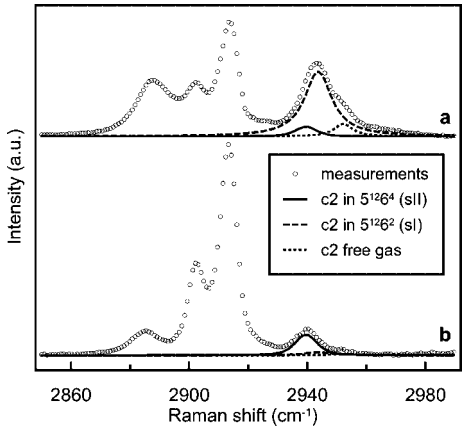

Figure 3. Raman spectra of methane−ethane hydrate in the vicinity of the gas/hydrate interface, and results of peak-fitting analysis for the higher-frequency C_2H_6 C−H stretching mode: (a) 65% CH_4 at 1 °C, 5.3 MPa without PVCap, 108 min after the first crystal was observed; (b) 93% CH_4 at 1 °C, 8.4 MPa without PVCap, 82 min after the first crystal was observed.

TABLE 1: Gaussian + Lorentzian Peak Parameters of the Higher-Frequency C−H Band of C_2H_6 in Methane−Ethane Gas Mixtures or Hydrate Cages, Obtained from the Reference Spectra (Figure 1)

	peak center (cm^{-1})	half-width (cm^{-1})	Lorentz %
in 65% CH_4 gas at 5.3 MPa	2953.9	7.5	96
in 93% CH_4 gas at 8.4 MPa	2953.4	8.0	99
in $5^{12}6^2$ hydrate cage (**sI**)	2945.4	11.2	100
in $5^{12}6^4$ hydrate cage (**sII**)	2941.3	8.8	53

TABLE 2: Induction Times for Hydrate Formation[a]

		induction time (min)
65% C1	first	84
	second	155
65% C1 with PVCap	first	128
	second	137
93% C1	first	72
	second	258
93% C1 with PVCap	first	394
	second	116

[a] Two repeat measurements were performed on fresh samples for each system.

3. Results

Induction Time. The induction times for hydrate formation were 84 and 155 min for the pure 65% C1 sample, 128 and 137 min for the 65% C1 sample with PVCap, 72 and 258 min for the pure 93% C1 sample, and 394 and 116 min for the 93% C1 sample with PVCap (Table 1). These observed induction times differed significantly between the repeat measurements, but this is due to the stochastic nature of the nucleation phenomenon. Note that the induction times were not reproducible for the same system. To compare the induction times between systems with statistical significance, a large number of measurements are needed.

Hydrate Structure in 65% C1 Samples. As discussed in this section, Raman analyses show that time-dependent hydrate structural change can be affected by the kinetic hydrate inhibitor. Figure 4 represents the methane−ethane hydrate structural compositions of the 65% CH_4 samples versus time after the first hydrate signals were observed. Only analyses of the first set of measurements are shown in Figure 4, because those of the repeat measurements were similar to the first ones (see Figure S1 in the Supporting Information). In these experiments, structure **I** hydrate is the thermodynamically stable state (calculated from CSMGem[18]). In the pure system (without PVCap), the formation of **sI** + **sII** hydrate mixtures with approximately 65% **sI** were observed (Figure 4a). Although the hydrate structure observed with Raman spectroscopy was dependent on the focal point of the laser used, there was no systematic change in the structure with time during the 6 h observation period (Figure 4a). These results suggest that the spatial distribution of the hydrate structure was not uniform, but the average composition remained almost unchanged during

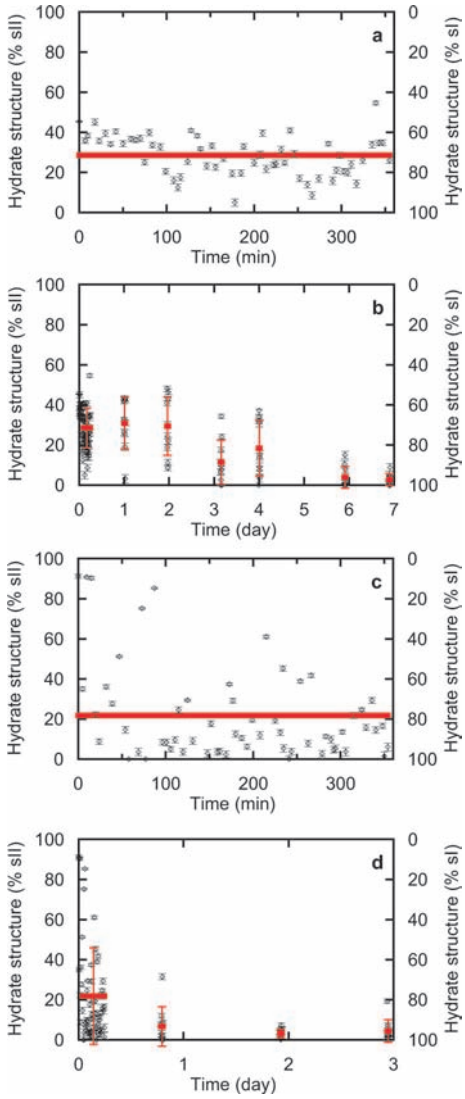

Figure 4. Methane-ethane hydrate structures at 1 °C and 5.3 MPa of 65% CH_4 in the vicinity of the gas/hydrate interfaces vs time after the first crystals were observed: (a) and (b) pure system; (c) and (d) system with 0.008 wt % PVCap. Red symbols represent the mean values for the duration of the observation.

the 6 h time period. In the longer time period observation (several days; Figure 4b), the average volume fraction of **sI** crystals in the hydrate phase was observed to increase with the elapse of time and attained almost 100% **sI** in 1 week, indicating the gradual hydrate structural conversion from metastable (**sII**) to stable structure (**sI**).

In the inhibited system with 0.008 wt % PVCap, the first hydrates observed were **sI** and **sII** mixtures, just like the case for the pure sample. However, the average signals from **sI** hydrate relative to those from **sII** hydrate were stronger than the pure sample (Figure 4c). The fraction of **sI** hydrate significantly increased on the time scale of hours (Figure 4c), and almost all hydrates observed 1 day after hydrate nucleation were **sI** crystals (Figure 4d). This suggests that the presence of PVCap promotes structural interconversion of metastable methane−ethane **sII** hydrate to stable methane−ethane **sI** hydrate.

Hydrate Structure in 93% C1 Samples. Trends in the structural conversion observed in the 93% CH_4 samples were different from those in the 65% CH_4 samples. Figure 5 represents the hydrate structural compositions of the 93% CH_4

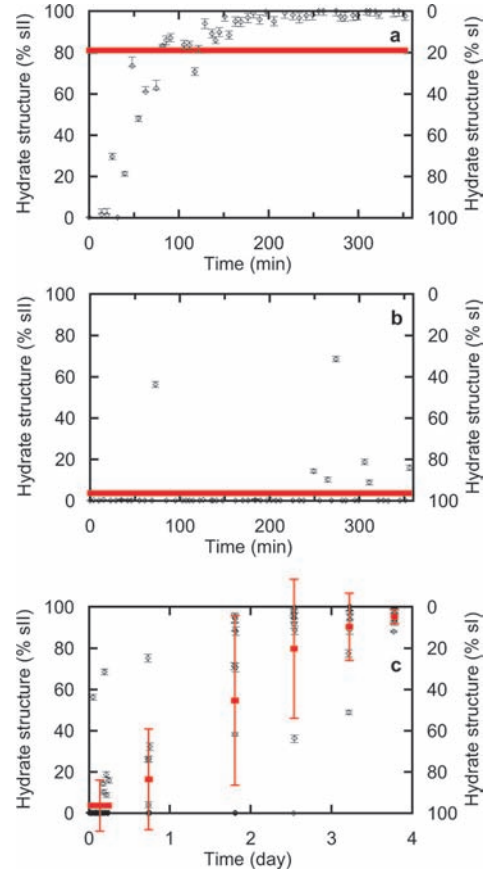

Figure 5. Methane−ethane hydrate structures at 1 °C and 8.4 MPa of 93% CH_4 in the vicinity of the gas/hydrate interfaces vs time after the first crystals were observed: (a) pure system; (b) and (c) system with 0.008 wt % PVCap. Red symbols represent the mean values for the duration of the observation.

samples measured as a function of time. Only analyses of the first set of measurements are shown in Figure 5, because those of the repeat measurements were similar to the first ones (see Figure S2 in Supporting Information). For these samples, the predicted stable hydrate structure was **sII** (calculated using CSMGem[18]). In the pure system without the inhibitor, hydrates initially observed were almost pure structure **I** crystals (Figure 5a). However, the fraction of **sI** hydrate rapidly decreased with time and was completely replaced by **sII** hydrate after approximately 3 h, indicating a fairly rapid interconversion compared with the 65% CH_4 sample (1 week).

On the other hand, for the system with 0.008 wt % PVCap, most of the measurements showed the presence of almost pure **sI** hydrate throughout the short-term observation (Figure 5b). Although structure **II** rich crystals were found in some measurements, the lack of observation of a systematic increase in the fraction of **sII** versus time indicates that considerable structural conversion did not occur in 6 h. During the long-term observation, the average **sII** fraction increased slowly with elapsed time and attained only about 95% after 4 days (Figure 5c). This indicates that it takes several days to complete the conversion to the stable structure **II** for the inhibited system, while the pure system converted to stable structure **II** within several hours. The finding that the structural conversion for the inhibited system proceeded much slower compared with the pure system indicates that PVCap considerably retards the structural transition in contrast to the results of 65% CH_4 (**sI**) samples.

Note that the hydrate structures observed were largely dependent on the focal point of the laser used in each

measurement (Figures 4 and 5). This fact implies that the hydrate structural transition propagates nonuniformly in a sample. The standard deviations of hydrate structural composition in the inhibited samples were greater than those for the pure systems, indicating that the presence of PVCap can increase the variability of the polymorph.

4. Discussion

The Cause of the Change in Hydrate Structure. There are two factors which can change hydrate structure at the interface: hydrate structural interconversion and growth of crystals with different structural composition on the top of the hydrate layer during the observations. Interconversion was considered to be the main cause of the observed change because considerable hydrate growth is not expected for the experiments. Taylor et al.[21] performed visual observations on clathrate hydrate film growth at the gas−water interface using video microscopy. They found that although a hydrate thin film grows to the thickness of tens of microns in the first 10 min after the nucleation, the film thickness remains almost unchanged on a time scale of hours. This result is explained by extremely slow crystal growth after the hydrate shell formation due to the gas and water transfer limitation by the presence of the solid layer barrier. Consistent with this, the thickness of the hydrate layer remained visibly unchanged after the first stage of hydrate formation in this present study, even after 7 days, suggesting no significant new hydrate growth.

Also, hydrate growth during the experiments may not account for the observed large differences in hydrate composition versus time profiles between the different systems. For example, in the systems without inhibitor present, the time required for the replacement of metastable crystals by a stable structure at 65% methane (Figure 4a and b) was 2 orders of magnitude longer compared with the 93% methane sample (Figure 5a). However, this cannot be reconciled with a correspondingly huge difference in hydrate growth rate between the two systems, because the same subcooling driving force for hydrate growth (of 14 °C subcooling) was used for both samples. The thermodynamic driving force is expressed as the difference in the chemical potential of liquid water and that of water in the hydrate phase, but it cannot explain the observations: the chemical-potential differences calculated by the statistical thermodynamics program CSMGem[18] are 411 J/mol for the 65% C1 samples and 347 J/mol for the 93% C1 samples, respectively.

Although the above observations support an interconversion process, we cannot completely rule out that some new hydrate growth contributed to the observed structural compositions.

Gas Composition Dependence of Methane−Ethane Hydrate Metastability. The results of the pure systems without the kinetic hydrate inhibitor (Figures 4b and 5a) show that the rate of structural conversion of hydrate mixtures in the 65% methane sample was 2 orders of magnitude slower than that in the 93% methane sample. These significant differences in structural conversion rates may be caused by possible differences in the following factors: (1) driving force for the structural transition and (2) kinetics of the interconversion.

Factor 1, the driving force, is likely to be a major factor because the driving forces estimated for the two systems predict a slower conversion in the 65% CH_4 sample, which is consistent with the observations. The differences in the chemical potential of water between the **sI** and **sII** systems calculated using CSMGem[18] are 36 J/mol for the 65% C1 sample and 66 J/mol for the 93% C1 sample, indicating that the driving force of the hydrate structural transition in the 65% C1 sample is lower than that in the 93% C1 sample.

Factor 2, the kinetics of interconversion, includes the mass transfer of guest molecules and water rearrangement for cage formation. Redistribution of guest gases in hydrate crystals is required for the structural transition, because the gas composition in **sI** hydrate is different from that in **sII** hydrate. CSMGem[18] can be used to estimate guest compositions in **sI** and **sII** crystals, i.e., (stable) **sI** contains 40% methane and (metastable) **sII** contains 66% methane for the 65% C1 gas mixture at 1 °C, 5.3 MPa; for the 93% C1 gas mixture at 1 °C, 8.4 MPa, (metastable) **sI** contains 78% methane and (stable) **sII** contains 76% methane. For the 65% methane gas mixture, there is a considerable difference in the guest compositions between the **sI** and **sII** hydrates, while the estimations for the two structures are about the same in the 93% methane gas mixture. This means that in the 65% methane system many more guest molecules have to redistribute when changing hydrate structure compared with the 93% methane system. This larger gas transportation may result in a slower structural transition rate.

Any water transport between **sI** and **sII** should be similar because water concentrations in **sI** and **sII** crystals are about the same. However, the crystalline water must break hydrogen bonds and rearrange to make the new cage structures during the interconversion of **sI** and **sII**. It seems reasonable to suppose that the energy for breaking the hydrogen bonding of the metastable cage structure is related to the energy barrier for the water rearrangement. Possible differences in hydrogen bonding strength between the two structures may result in significantly different activation energies for the reaction, although there is currently insufficient knowledge in the literature to discuss this phenomenon on a molecular scale.

From above arguments, we conclude that the differences in both the driving force and the kinetics for the interconversion can explain the different transition rates observed between the two systems.

Effect of PVCap on the Hydrate Structural Conversion. Our Raman analyses of hydrate structures show that the presence of PVCap affects the metastability of the methane−ethane hydrates (Figures 4 and 5). It is well-known that hydrate formation is significantly retarded by the addition of PVCap;[14,22] however, this is the first time that the kinetic hydrate inhibitor has been shown to influence the hydrate structural transition.

Larsen et al.[23] proposed that PVCap adsorbs onto hydrate surfaces through hydrogen bonding. As a result of surface pinning by the adsorbent, crystal surfaces have microcurvatures, resulting in crystal-growth inhibition due to the Gibbs−Thomson (Kelvin) effect. The adsorption of PVCap to hydrate surfaces was observed using small-angle neutron scattering,[24] which was also supported by molecular simulations.[25,26] Assuming that adsorption of PVCap occurred in our experiments, adsorbed polymers may disturb the gas capture or release and water rearrangement at crystal interfaces, which are essential for the structural conversion as discussed above. This idea can account for the inhibition of the interconversion by PVCap observed in the 93% methane samples (**sII**) qualitatively. However, the explanation of the opposite tendency of promotion of the structural transition by the inhibitor found in the 65% methane samples (**sI**) is unclear. Although it is known that kinetic inhibitors retard the hydrate nucleation and affect subsequent growth in most cases,[14,22] results of gas consumption measurements on carbon dioxide hydrate formation[27] suggested that poly(*N*-vinylpyrrolidone) (PVP) delays the nucleation but promotes crystal growth; more recently Lee and Englezos[28]

found in their visual observation of methane−ethane hydrate formation that when inhibitors GHI 101 were present, the nucleation inhibition was followed by catastrophic crystal growth. These diverse actions of kinetic inhibitors imply the existence of complicated interactions between polymers, water, and gases at crystal surfaces which may depend on hydrate structure and guest composition. To answer the questions, *in situ* observation of the hydrate surface phenomena, for example by using small-angle neutron scattering,[24,29] may be required. Understanding the probable difference in the structure of adsorbed polymers and crystal interfaces between the inhibited and promoted systems will provide important clues to clarify the fundamental mechanism of kinetic hydrate inhibition.

5. Conclusions

In order to understand methane−ethane hydrate metastability, structures of hydrates formed from liquid water and methane−ethane gas mixtures have been measured as a function of time after the first hydrate crystals were observed using Raman spectroscopy. To investigate the effect of gas composition and the presence of a kinetic hydrate inhibitor on hydrate metastability, two methane−ethane gas mixtures of 65% or 93% CH_4 and water, with and without inhibitors (0.008 wt % PVCap), have been studied.

Initially, mixtures of **sI** and **sII** formed in all experiments, and the subsequent conversion from metastable to stable structures, were observed. It was found that the degree of metastability depends on gas composition. When the results of the pure systems are compared, at 65% CH_4 the two structures coexisted for 1 week, while at 93% CH_4 Raman signals from **sI** (metastable) quickly weakened and disappeared in a few hours, indicating that the structural conversion is much faster at the higher concentration of CH_4. This discrepancy can be explained as the differences in the driving force and kinetics of the interconversion, namely, difference in the chemical potential of water in **sI** and **sII** hydrate, the degree of guest-gas redistribution, and activation energy for water rearrangement. Also, it was found that the presence of PVCap affects the metastability: at 65% CH_4 the inhibited system had less metastable **sII** than the pure system, while at 93% CH_4 the conversion rate was 2 orders of magnitude slower than the pure system.

These findings have potentially important implications in pipeline flow assurance and in crystal growth processes in general.

Acknowledgment. The present study is supported by the ACS Petroleum Research Fund (no. 42254-AC2).

Supporting Information Available: Results of supplementary tests (Figures S1 and S2). This information is available free of charge via the Internet at http://pubs.acs.org.

References and Notes

(1) Sloan, E. D., Jr.; Koh, C. A. *Clathrate Hydrates of Natural Gases*, 3rd ed.; CRC Press−Taylor and Francis: Boca Raton, FL, 2008.
(2) Sloan, E. D., Jr *Energy Fuels* **1998**, *12*, 191.
(3) Koh, C. A. *Chem. Soc. Rev.* **2002**, *31*, 157.
(4) Sloan, E. D., Jr *Nature* **2003**, *426*, 353.
(5) Koh, C. A.; Sloan, E. D., Jr *AIChE J.* **2007**, *53*, 1636.
(6) Ballard, A. L.; Sloan, E. D., Jr *Chem. Eng. Sci.* **2000**, *55*, 5773.
(7) Hendriks, E. M.; Edmonds, B.; Moorwood, R. A. S.; Szczepanski, R. *Fluid Phase Equilib.* **1996**, *117*, 193.
(8) Subramanian, S.; Kini, R. A.; Dec, S. F.; Sloan, E. D., Jr *Chem. Eng. Sci.* **2000**, *55*, 1981.
(9) Subramanian, S.; Ballard, A. L.; Kini, R. A.; Dec, S. F.; Sloan, E. D., Jr *Chem. Eng. Sci.* **2000**, *55*, 5763.
(10) Ripmeester, J. A. *Ann. N. Y. Acad. Sci.* **2000**, *912*, 1.
(11) Hester, K.; Sloan, E. D., Jr *Int. J. Thermophys.* **2005**, *26*, 95.
(12) Takeya, S.; Kamata, Y.; Uchida, T.; Nagao, J.; Ebinuma, T.; Narita, H.; Hori, A.; Hondoh, T. *Can. J. Phys.* **2003**, *81*, 479.
(13) Bowler, K. E.; Stadterman, L. L.; Dec, S. F.; Koh, C. A.; Sloan, E. D., Jr.; Creek, J. L. *Proc. 5th Int. Conf. Gas Hydrates* **2005**, *5*, 5030.
(14) Kelland, M. A. *Energy Fuels* **2006**, *20*, 825.
(15) Subramanian, S. Ph.D. Thesis, Colorado School of Mines, 2000.
(16) Hester, K. C. Ph.D. Thesis, Colorado School of Mines, 2007.
(17) Uchida, T.; Takeya, S.; Kamata, Y.; Ikeda, I. Y.; Nagao, J.; Ebinuma, T.; Narita, H.; Zatsepina, O.; Buffett, B. A *J. Phys. Chem. B* **2002**, *106*, 12426.
(18) Ballard, A. L.; Sloan, E. D., Jr *Fluid Phase Equilib.* **2002**, *371*, 194.
(19) Ohno, H.; Dec, S. F.; Sloan, E. D., Jr.; Koh, C. A. *Proc. 6th Int. Conf. Gas Hydrates*, submitted.
(20) Moudrakovski, I. L.; Sanchez, A. A.; Ratcliffe, C. I.; Ripmeester, J. A. *J. Phys. Chem. B* **2001**, *105*, 12338.
(21) Taylor, C. J.; Miller, K. T.; Koh, C. A.; Sloan, E. D., Jr *Chem. Eng. Sci.* **2007**, *62*, 6524..
(22) Lederhos, J. P.; Long, J. P.; Sum, A.; Christiansen, R. L.; Sloan, E. D., Jr *Chem. Eng. Sci.* **1996**, *51*, 1221.
(23) Larsen, R.; Knight, C. A.; Sloan, E. D., Jr *Fluid Phase Equilib.* **1998**, *150−151*, 353.
(24) King, H. E., Jr.; Hutter, J. L.; Lin, M. Y.; Sun, T. *J. Chem. Phys.* **2000**, *112*, 2523.
(25) Carver, T. J.; Drew, M. G. B.; Rodger, P. M. *J. Chem. Soc., Faraday Trans.* **1995**, *91*, 3449.
(26) Anderson, B. J.; Tester, J. W.; Borghi, G. P.; Trout, B. L. *J. Am. Chem. Soc.* **2005**, *127*, 17852.
(27) Motie, R. E. Ph.D. Thesis, King's College London, 1998.
(28) Lee, J. D.; Englezos, P. *Chem. Eng. Sci.* **2006**, *61*, 1368.
(29) Hutter, J. L.; King, H. E., Jr.; Lin, M. Y. *Macromolecules* **2000**, *33*, 2670.

JP8010603